

# Large Eddy Simulations of the Flow in a Three-Dimensional Ventilated Room

Lars Davidson\*  
Thermo and Fluid Dynamics  
Chalmers University of Technology  
S-412 96 Gothenburg, Sweden  
E-mail: lada@tfd.chalmers.se

Peter V. Nielsen  
Dep. of Building Technology and Structural Engineering  
Aalborg University  
Sohngaardsholmsvej 57  
DK-9000 Aalborg, Denmark  
E-mail: i6pvn@civil.auc.dk

## ABSTRACT

We have done Large Eddy Simulations (LES) of the flow in a three-dimensional ventilated room.

A finite volume method is used with a collocated grid arrangement. The momentum equations are solved with an explicit method using central differencing for all terms. The pressure is obtained from a Poisson equation, which is solved with a conjugate gradient method. For the discretization in time we use the Adam-Bashfourth scheme, which is second-order accurate.

When using LES, the time-dependent three-dimensional momentum and continuity are solved. A subgrid turbulence model is used to model the turbulent scales which are smaller than the cells. We have used two different subgrid models: the traditional Smagorinsky model, and the dynamic model of Germano. Instead of the traditional time averaging, the equations when using LES are *filtered* in space, and  $\bar{u}_i$  is a function of space and time.

With LES we get much more information than when using traditional time averaged turbulence models, since we are resolving most of the turbulence. It is found that the instantaneous fluctuations are very large. For example, in the region of the wall jet below the ceiling where the time averaged velocity  $\langle \bar{u} \rangle / U_0$  is typically 0.5, the instantaneous velocity fluctuates between 0.3 and 0.8.

---

\*This work was carried out during the author's stay at Dep. of Building Technology and Structural Engineering, Aalborg University in Autumn 1995.

## 1 INTRODUCTION

The Navier-Stokes equations are traditionally studied in their time-averaged form, often referred to as the Reynolds equations. The resulting unknown stresses  $\overline{u_i u_j}$  stemming from the time averaging needs to be modelled with a turbulence model. The most common turbulence model is the two-equation  $k - \varepsilon$  model [12]. In industry today, the  $k - \varepsilon$  model is routinely used and the model is included in most commercial CFD-packages. The advantage of the  $k - \varepsilon$  model from a numerical point of view is that it is robust and reliable. From a physical point of view the physics is treated in a simplistic manner, but nevertheless the model works surprisingly well in many types of flows.

However, there are physical phenomena which eddy viscosity models like the  $k - \varepsilon$  model cannot capture such as streamline curvature and the effect of irrotational strains. Reynolds Stress Models (RSM) [8] do take this effects into account [1, 2]. RSMs have been proven to be able to predict a number of types of flows better than  $k - \varepsilon$  models. For a review, see Refs. [11, 13, 9]. Also Reynolds Stress Models are incorporated in many commercial CFD-codes, and RSMs are being increasingly used in the industry.

There seems to be a number of flows where the time averaged Navier-Stokes equations cannot be used, because too much information is filtered out in the time averaging process. Examples are transitional flows, either free or wall bounded, and separated flows where it is not appropriate to use the concept "mean" and "fluctuating" velocities as

they are both of the same magnitude [22]. Flows around and behind bluff bodies is another example where the “mean” flow is not steady. These types of flows can probably be successfully predicted by Large Eddy Simulations (LES). It can be interesting to use LES also in ventilated rooms, where the turbulent fluctuations often are very large. In LES most of these scales are resolved.

In the next section the subgrid models are described. The following sections presents and discusses the results, and in the final section we draw some conclusions and discuss future work.

## 2 LARGE EDDY SIMULATIONS

### 2.1 Equations

With a spatial, inhomogeneous filter (denoted by a bar) applied to the incompressible Navier-Stokes equations, we obtain the momentum and continuity equations for the large scale motion

$$\frac{\partial \bar{u}_i}{\partial t} + \frac{\partial}{\partial x_j} (\bar{u}_i \bar{u}_j) = -\frac{1}{\rho} \frac{\partial \bar{p}}{\partial x_i} + \nu \frac{\partial^2 \bar{u}_i}{\partial x_j \partial x_j} - \frac{\partial \tau_{ij}}{\partial x_j} \quad (1)$$

$$\frac{\partial \bar{u}_i}{\partial x_i} = 0 \quad (2)$$

where the subgrid stresses are given by

$$\tau_{ij} = \overline{u_i u_j} - \bar{u}_i \bar{u}_j \quad (3)$$

### 2.2 Subgrid Models

We need a subgrid model to model the turbulent scales which cannot be resolved by the grid. In the present study we have chosen to use two types of models:

1. The simple model of Smagorinsky [21]
2. A dynamic subgrid model of Germano [6]

#### 2.2.1 The Smagorinsky Model

The Smagorinsky model can be written [21]

$$\tau_{ij} - \frac{1}{3} \delta_{ij} \tau_{kk} = -2\nu_T \bar{S}_{ij} \quad (4)$$

$$\nu_T = (C_S \Delta)^2 \sqrt{2 \bar{S}_{ij} \bar{S}_{ij}} \quad (5)$$

where  $-\frac{1}{3} \delta_{ij} \tau_{kk}$  is included on the left-hand side to make the equation to be valid upon contraction

(setting the indices  $i$  and  $j$  equal). The strain tensor  $\bar{S}_{ij}$  is defined as

$$\bar{S}_{ij} = \frac{1}{2} \left( \frac{\partial \bar{u}_i}{\partial x_j} + \frac{\partial \bar{u}_j}{\partial x_i} \right) \quad (6)$$

and the filter-width is taken as the local grid size, i.e.

$$\Delta = (\Delta_{x,i} \Delta_{y,j} \Delta_{z,k})^{1/3} \equiv (\Delta V_{ijk})^{1/3} \quad (7)$$

where indices  $i, j, k$  denote cell-index in the three coordinate directions, and  $\Delta V_{ijk}$  is the volume of the computational cell  $i, j, k$ .

Often a damping function is applied to the turbulent viscosity to account for viscous effects near walls. A standard form is chosen in this study which reads [23]

$$f_\mu = 1 - \exp\left(-\frac{n^+}{25}\right) \quad (8)$$

where  $n^+ = u_* n / \nu$  ( $u_*$  and  $n$  denote friction velocity and normal wall distance, respectively).

The disadvantage of this model is that the constant  $C_S$  is unknown, and that it influences the calculated results very much. In the literature, the constant is found to vary in the range from  $C_S = 0.065$  [15] to  $C_S = 0.25$  [10].

#### 2.2.2 The Dynamic Subgrid Model

Germano *et al.* [6, 7] propose a *dynamic* subgrid model in which the constant  $C$  is not arbitrarily chosen (or optimized), but where it is *computed*. For convenience, the derivation of the Dynamic Subgrid Model given in Ref. [6] is repeated below. A second, coarser filter (test filter, denoted by  $\widehat{\cdot}$ ) is applied to the equations. This size of the test filter (denoted by  $\widehat{\Delta}$ ) is twice as coarse as the grid filter ( $\Delta$ ). When applying this second filter to Eq.1, we obtain

$$\begin{aligned} & \frac{\partial \widehat{u}_i}{\partial t} + \frac{\partial}{\partial x_j} (\widehat{u}_i \widehat{u}_j) \\ &= -\frac{1}{\rho} \frac{\partial \widehat{p}}{\partial x_i} + \nu \frac{\partial^2 \widehat{u}_i}{\partial x_j \partial x_j} - \frac{\partial T_{ij}}{\partial x_j} \end{aligned}$$

where the subgrid stresses now are given by

$$T_{ij} = \overline{\widehat{u}_i \widehat{u}_j} - \widehat{u}_i \widehat{u}_j \quad (9)$$

Consider the resolved turbulent stresses  $\mathcal{L}_{ij}$  defined as

$$\mathcal{L}_{ij} = \overline{\widehat{u}_i \widehat{u}_j} - \widehat{u}_i \widehat{u}_j \quad (10)$$

which is representative of the contribution to the Reynolds stresses by the scales  $\ell$  in the range between  $\Delta$  and  $\widehat{\Delta}$ , i.e.  $\Delta < \ell < \widehat{\Delta}$ . From Eqs. 3,9,10 we obtain

$$\mathcal{L}_{ij} = T_{ij} - \widehat{\tau}_{ij} \quad (11)$$

Assume now that the functional form we use for the subgrid stresses for the  $\tau_{ij}$  in the Smagorinsky model in Eq. 4 (grid filter level), also can be used to relate the subgrid stresses  $T_{ij}$  to  $\widehat{\Delta}$  and  $\widehat{S}_{ij}$  at the test filter level. Combining Eqs. 4,5, we can write (note that while the Smagorinsky constant  $C_S$  in Eq.5 is squared,  $C$  is not)

$$\tau_{ij} - \frac{1}{3}\delta_{ij}\tau_{kk} = -2C\Delta^2|\widehat{S}|\widehat{S}_{ij} \quad (12)$$

$$T_{ij} - \frac{1}{3}\delta_{ij}T_{kk} = -2C\widehat{\Delta}^2|\widehat{S}|\widehat{S}_{ij} \quad (13)$$

where

$$|\widehat{S}| = \sqrt{2\widehat{S}_{ij}\widehat{S}_{ij}}, \quad \widehat{S}_{ij} = \frac{1}{2} \left( \frac{\partial \widehat{u}_i}{\partial x_j} + \frac{\partial \widehat{u}_j}{\partial x_i} \right) \\ |\widehat{S}| = \sqrt{2\widehat{S}_{ij}\widehat{S}_{ij}} \quad (14)$$

Applying the test filter to Eq.12, substituting this equation and Eq.13 into Eq.10 gives

$$\mathcal{L}_{ij} - \frac{1}{3}\delta_{ij}\mathcal{L}_{kk} = \\ -2C \left( \widehat{\Delta}^2|\widehat{S}|\widehat{S}_{ij} - \Delta^2|\widehat{S}|\widehat{S}_{ij} \right) \quad (15)$$

Note that the ‘‘constant’’  $C$  really is a function of both space and time, i.e.  $C = C(x_i, t)$ . When deriving Eq.15 it has been assumed that the variation of  $C$  in space is slow, which allowed us to treat  $C$  as constant when applying the test filter to Eq.12.

Equation 15 is a tensor equation, which means that we have five ( $S_{ij}$  is symmetric and its trace is zero) equations for  $C$ . Germano *et al.* proposed to contract Eq. 15 with  $\widehat{S}_{ij}$  in order to reduce it to one equation. Later, Lilly [14] suggested to satisfy Eq. 15 in a least-square sense gives

$$C = \frac{\mathcal{L}_{ij}M_{ij}}{2M_{ij}M_{ij}} \quad (16)$$

For more details see [3]

### 2.3 Numerical Procedure

Equations 1 are solved with a finite volume procedure. Initially we tried to use an implicit SIMPLE code [4], but it turned out to be too expensive.

In SIMPLE methods, one must iterate between the momentum equations and the pressure correction equation, and this required some twenty iterations on each time step, even though the CFL number

$$CFL = \max \left\{ \frac{\Delta t}{\Delta t_{conv}}, \frac{\Delta t}{\Delta t_{diff}} \right\}$$

$$\Delta t_{conv} = \min \left\{ \frac{\Delta x}{\bar{u}}, \frac{\Delta y}{\bar{v}}, \frac{\Delta z}{\bar{w}} \right\}$$

$$\Delta t_{diff} = \rho \frac{\min \{ (\Delta x)^2, (\Delta y)^2, (\Delta z)^2 \}}{\mu + \mu_t}$$

was kept well below one. After that we started to work on an explicit method. For more details see Ref. [3].

We want to solve Eqs.1. The convection and diffusion terms are discretized using a finite volume method [4, 17] on a collocated grid. Second-order central differencing is used for both convection, diffusion and stresses. It has been found that the QUICK scheme is too dissipative in connection with LES. The momentum equations are solved explicitly and we have an implicit Poisson equation for the pressure which must be solved each time step. In the present work it is solved with a conjugate gradient method with an incomplete Cholesky factorization as a preconditioner. The solver is a part of the SLAP package (Sparse Linear Algebra Package) available on `netlib`. This solver was implemented by Renard and Gresser [18]. For more details see Ref. [3]

### 2.4 Boundary Conditions

For the pressure we use Neumann conditions at all boundaries, i.e.

$$\frac{\partial \bar{p}}{\partial n} = 0 \quad (17)$$

where  $n$  is the coordinate direction normal to the boundary. No-slip conditions is used for the velocities  $\bar{u}_i$ .

When using grids which are coarse near the floor (the  $72 \times 42 \times 52$  mesh and the  $102 \times 52 \times 52$ ) we use wall functions at the walls [4]. When the distance between the wall and the near-wall node exceeds 11 viscous units ( $n^+ = 11$ ), the viscosity at the wall is set from the law of the wall [4], which corresponds to prescribing a wall shear stress  $\tau_w$  according to the law of the wall.

## 3 RESULTS

The explicit code described in Sub-section 2.3 is used. A steady computation is first carried out us-

ing the CALC-BFC code and the  $k - \varepsilon$  mode [3]. These results are used as initial start fields in the LES calculations. The number of time steps used in each calculation is typically 40000, which for the  $72 \times 42 \times 26$  is approximately 900 seconds when using the dynamic model. The streamwise average of the peak velocity in the wall jet along the ceiling is close to  $U_{av} = 0.5U_{in}$  ( $= 0.228$  m/s). Thus the time it takes for fluid particle to move from the inlet to the opposite wall can be estimated as  $L/U_{av} \simeq 40$  seconds, which means that  $900/40 \simeq 22.5$  characteristic time units ( $L/U_{av}$ ) are covered in a simulation. The predictions are compared with experiments of Restivo [19] (also available in Ref. [16])

Since we resolve the large-scale turbulence we should impose turbulent flow conditions at the inlet. As an approximation random fluctuations are superimposed on the time-averaged experimental flow conditions at the inlet according to:

$$\begin{aligned} \bar{u}_{in} &= U_{in} + random \cdot u'_{exp}, \quad \bar{v}_{in} = random \cdot u'_{exp} \\ \bar{w}_{in} &= random \cdot u'_{exp} \end{aligned} \quad (18)$$

Note that the random function is called at different times for  $\bar{u}_{in}$ ,  $\bar{v}_{in}$  and  $\bar{w}_{in}$ , which means that the fluctuations are not correlated. This means, furthermore, that the shear stresses  $\overline{u'v'}$ ,  $\overline{u'w'}$  and  $\overline{v'w'}$ , become zero at the inlet.

The maximum CFL number is, for stability reasons, set to 0.4.

### 3.1 Using the Smagorinsky Model

In Fig. 1 the time averaged ( $\langle \cdot \rangle_t$  denotes time averaging) predicted velocity profiles are compared with experiments. Prediction with two different values on the constant  $C_S$  are shown in Fig. 1, and as can be seen the solutions differ considerable. Thus it seems that when using this model the constant  $C_S$  must first optimized, and this value is probably both flow dependent as well as grid dependent. This is the reason why this model was abandon in the present work and attention was shifted to the dynamic model.

### 3.2 Using the Dynamic Model

Three different meshes have been used:  $72 \times 52 \times 26$ ,  $72 \times 42 \times 52$  and  $102 \times 52 \times 52$ . For all three meshes geometrical stretching is used in  $y$ -direction, and a hyperbolic tangent function is used in  $x$  and  $z$ -direction.

It is well known that when using the dynamic model one must set some limits on  $C$  in Eq. 16 or do some averaging in order to achieve numerical stability. In the present study we average  $C$  in

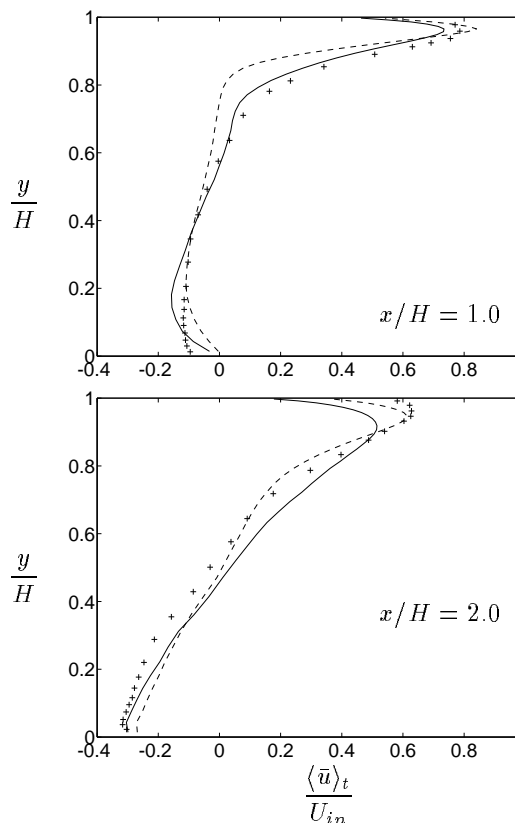


Figure 1: Time averaged velocity profiles. Symmetry plane  $z/H = 0.5$ . LES using the Smagorinsky model. Mesh:  $72 \times 52 \times 26$ . Solid lines:  $C_S = 0.14$ ; dashed lines:  $C_S = 0.18$ ; +: experimental  $U/U_{in}$ .

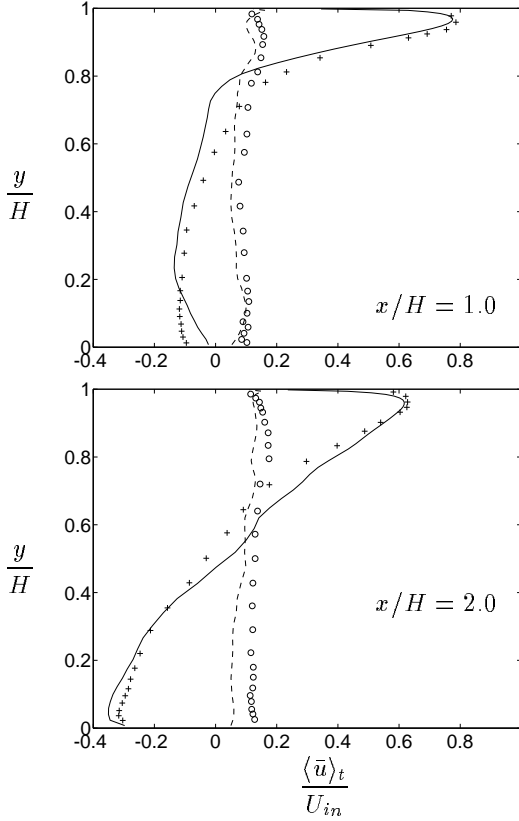


Figure 2: Time averaged velocity and rms velocity profiles.  $102 \times 52 \times 52$  mesh. Symmetry plane  $z/H = 0.5$ . LES using the dynamic model. Solid lines:  $\langle \bar{u} \rangle_t / U_{in}$ ; dashed lines:  $u_{rms} / U_{in}$ ; +: experimental mean velocity; o: experimental fluctuations.

the spanwise ( $z$ ) direction. This was found not to be enough. In addition we had to average  $C$  in  $x$  ( $i = \pm 2$ ) and  $y$ -direction ( $j = \pm 2$ ). Furthermore the total (laminar plus turbulent) viscosity is not allowed to become negative. No maximum limit on  $C$  (or viscosity) was used. This procedure is similar to that chosen in Ref. [24].

When comparing with experiments we must time average over a certain time  $T$  in the same way experimentalists measure over a certain time when they are recording a turbulent signal. The question is when we should start to time average ( $T_0$ ) and for how long ( $T$ ). In [3] we investigated the influence of  $T_0$  and  $T$  on the time averaged  $\bar{u}$ -profile. In general the  $\langle \bar{u} \rangle_t$  does not seem to be very sensitive to the choice of  $T$  and  $T_0$ , but the differences are largest close to  $y/H = 0.5$ . This has also been found in experimental investigations, where longer measuring times must be used in the middle of the room (low-speed regions) than near walls (high-speed regions)<sup>1</sup> In [3] it was shown that when reducing the time averaging to the first

<sup>1</sup>Hyldgård, C.E., private communication, Dep. of Building Technology and Structural Engineering, Aalborg University

10000 time steps the magnitude of  $\langle \bar{u} \rangle_t$  starts to increase close to the floor.

In [3] the predicted velocity profiles using the three different meshes were compared with experiments. It was found that the agreement with experiments was fairly good for all meshes, but that the solutions are grid dependent. In general the resolved rms fluctuations

$$u''(t) = \bar{u}(t) - \langle \bar{u}(t) \rangle_t, \quad u_{rms} = \sqrt{\langle (u''(t))^2 \rangle_t}$$

were under-predicted. In Fig. 2 the predictions on the fine mesh are shown.

The  $\langle \bar{u} \rangle_t$  profiles along the ceiling (at  $y = H - y/2$ ) and the floor (at  $y = y/2$ ) are shown in Fig. 3. The agreement between predictions and experiments is fairly good. The recirculation bubble along the ceiling close to the opposite wall is over-predicted compared to experiments. Furthermore it can be seen that there is a large difference in the flow along the floor when using the two grids. The coarse grid severely under-predicts the  $\langle \bar{u} \rangle_t$  velocity. The fine grid gives a much closer agreement with experiments. However, the fine grid predicts a separation along the floor at  $x/H \simeq 1.2$  which is too early according to experimental data. Downstream ( $0.3 < x/H < 1.2$ ) there is a stagnant region with  $\langle \bar{u} \rangle_t$  velocities close to zero.

The resolved  $\bar{u}$  velocities versus time at three chosen points are presented in Fig. 4. It can be seen that the fluctuations in  $\bar{u}$  are strong. In the middle of the room (Fig. 4b) it is not meaningful to define a “mean” velocity  $\langle \bar{u} \rangle_t$ , since  $\bar{u}/U_{in}$  fluctuates between 0.15 and -0.23 and the time averaged velocity is close to zero. It can also be seen that the frequency of  $\bar{u}$  is much higher in the wall jet near the ceiling (Figs. 4a) than in the back-flow region close to the floor (Fig. 4c). In addition to the large-scale fluctuations visible in Fig. 4 we have small-scale fluctuations (see [3]). These small-scale fluctuations are generated by the inlet boundary conditions, where a randomized velocity field is prescribed (see Eq. 18). If constant flow conditions (in time) are prescribed, the small-scale fluctuations go away. Also the time history of the  $\bar{u}$  velocities (like that shown in Fig. 4) becomes less chaotic.

The probability density function of  $\bar{u}$  is shown for four points in Fig. 5, two points in the wall jet and two points in the boundary layer close to the floor. For the points in the wall jet (Fig. 5a) the probability function show a preferred value of  $\bar{u}$  showing that the flow has a well defined mean velocity and that the velocity is fluctuating around this mean value. Close to the floor near the separation at  $x/H = 2$  (Fig. 5b) it is hard to find any preferred value of  $\bar{u}$  which shows that the flow is irregular and unsta-

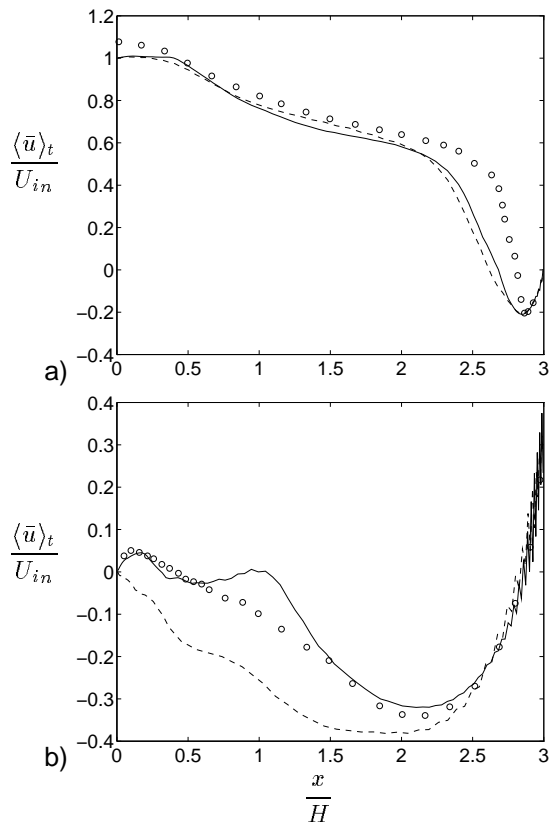


Figure 3: Time averaged  $\bar{u}$  velocity along the ceiling and the floor. The dynamic model.  $z/H = 0.5$ . Solid line:  $102 \times 52 \times 52$  mesh; dashed lines:  $72 \times 52 \times 26$  mesh;  $\circ$ : experiments. a)  $y = H - h/2$ . b)  $y = h/2$ .

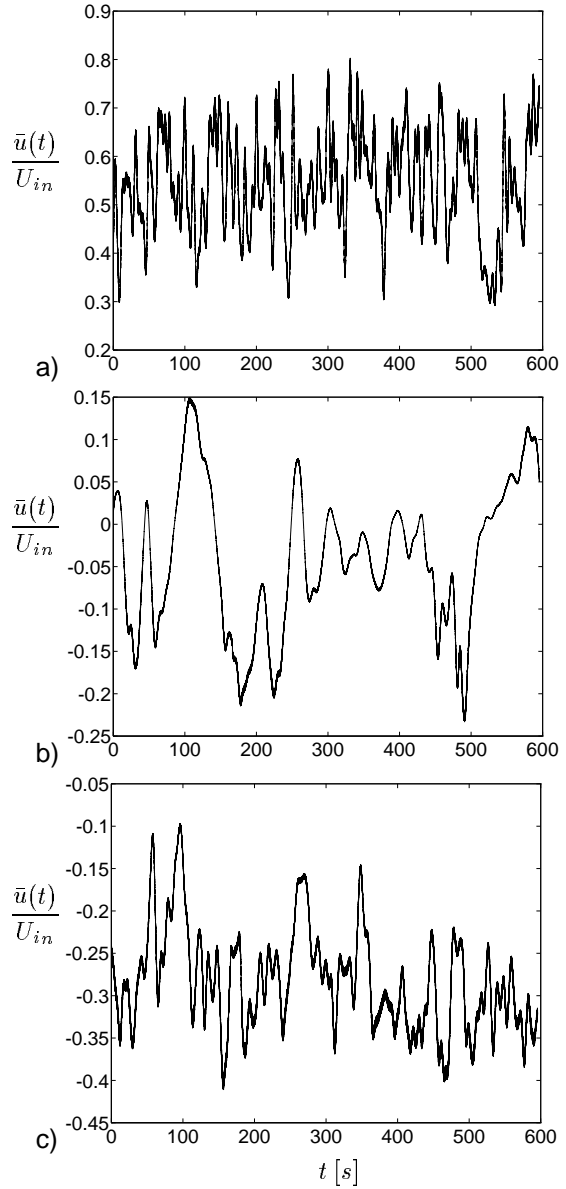


Figure 4: Time history of the  $\bar{u}$  at three chosen cells.  $72 \times 52 \times 26$  mesh.  $z/H = 0.5$ . Dynamic model. a)  $x/H = 2.0, y/H = 0.92$ ; b)  $x/H = 1.0, y/H = 0.5$ ; c)  $x/H = 2.0, y/H = 0.14$ .

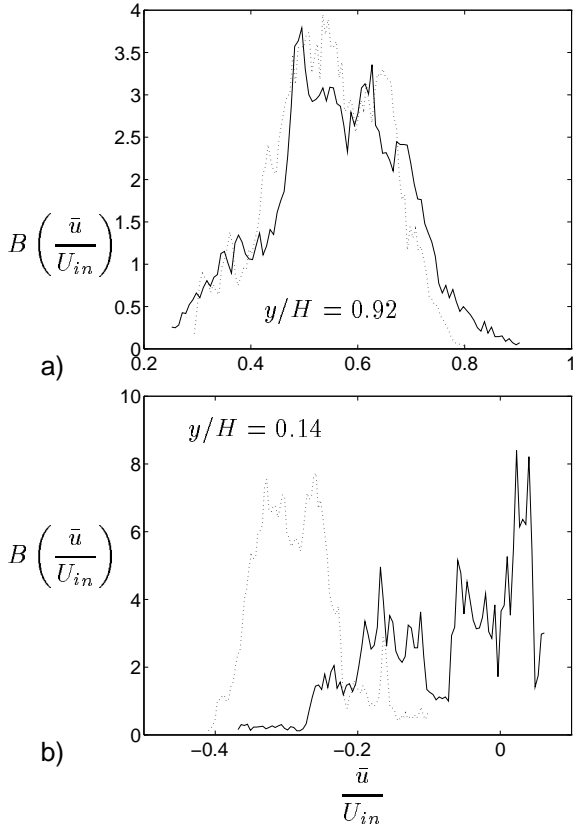


Figure 5: Probability density function of  $\bar{u}$ .  $72 \times 52 \times 26$  mesh. The dynamic model. a) Solid line:  $x/H = 1.0$ ; dotted line:  $x/H = 2.0$ . b) Solid line:  $x/H = 1.0$ ; dotted line:  $x/H = 2.0$ ;

ble with no well defined mean velocity and large fluctuations.

In Fig. 6 the power density spectrum for the resolved streamwise fluctuation  $(u'')^2$  is shown. In fully turbulent flow it should behave as  $\Phi \propto n^{-5/3}$  (inertial region) which is included as a dashed line. We can see that there is some tendency to inertial region close to  $f = 0.2$ . This value agrees well with measurements by Sandberg [20]. The sharp decrease of  $\Phi$  shows that the subgrid model is doing a good job in extracting energy from the resolved flow. The reason why we do not have any distinct inertial region in the spectra may well be connected to insufficient grid resolution.

## 4 CONCLUSIONS AND FUTURE WORK

A numerical procedure for Large Eddy Simulations has been presented for prediction of recirculating flows. A simple Smagorinsky model and a dynamic model was tested. The following conclu-

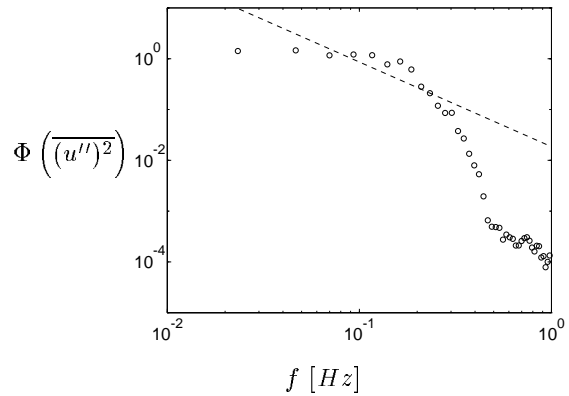


Figure 6: Power density spectrum  $\Phi \left( \overline{(u'')^2} \right)$ .  $72 \times 52 \times 26$  mesh. Dynamic model. Symmetry plane  $z/H = 0.5$ .  $x/H = 2.0$ ,  $y/H = 0.92$ .

sions can be drawn:

- The simple Smagorinsky model was found to be inadequate, because the results were very dependent on the Smagorinsky-constant
- The pressure equation requires some 80 % of the total CPU-time
- The results obtained with the dynamic subgrid model gives results in good agreement with experiments

### 4.1 Future Work

In an ongoing work [5] we have found the multigrid solver solves the pressure equations more than 10 times faster on fine meshes (1 million nodes). We are also working on solving the whole equation system *implicitly* [5] using the same multigrid solver for the pressure. In the explicit method used in the present work the CFL-number must for stability reasons be below 0.4. With an implicit method the CFL-number is restricted only by concern of accuracy. Using CFL-number of one the implicit method is somewhat faster than the explicit method. If the CFL-number is allowed locally to exceed one (say 2), the implicit method gives a further speed-up of more than two.

## References

- [1] DAVIDSON, L. Prediction of the fbw around an airfoil using a Reynolds stress transport model. *ASME J. Fluid Engng.* 117 (1995), 50–57.
- [2] DAVIDSON, L. Reynolds stress transport modelling of shock-induced separated fbw. *Computers & Fluids* 24 (1995), 253–268.

- [3] DAVIDSON, L. Implementation of a large eddy simulation method applied to recirculating flow in a ventilated room. Report, ISSN 1395-7953 R9611, Dep. of Building Technology and Structural Engineering, Aalborg University, 1996.
- [4] DAVIDSON, L., AND FARHANIEH, B. CALC-BFC: A finite-volume code employing collocated variable arrangement and cartesian velocity components for computation of fluid flow and heat transfer in complex three-dimensional geometries. Rept. 92/4, Thermo and Fluid Dynamics, Chalmers University of Technology, Gothenburg, 1992.
- [5] EMVIN, P., AND DAVIDSON, L. Development and implementation of a fast large eddy simulations method. Report (in press), Thermo and Fluid Dynamics, Chalmers University of Technology, Gothenburg, 1996.
- [6] GERMANO, M., PIOMELLI, U., MOIN, P., AND CABOT, W. A dynamic subgrid-scale eddy viscosity model. *Phys. Fluids A* 3 (1991), 1760–1765.
- [7] GERMANO, M., PIOMELLI, U., MOIN, P., AND CABOT, W. Erratum. *Phys. Fluids A* 3 (1991), 3128.
- [8] GIBSON, M., AND LAUNDER, B. Ground effects on pressure fluctuations in the atmospheric boundary layer. *J. Fluid Mech.* 86 (1978), 491–511.
- [9] HANJALIĆ, K. Advanced turbulence closure models: A view of current status and future prospects. *Int. J. Heat and Fluid Flow* 15 (1994), 178–203.
- [10] JONES, W., AND WILLE, M. Large eddy simulation of a jet in a cross-flow. In *10th Symp. on Turbulent Shear Flows* (The Pennsylvania State University, 1995), pp. 4:1 – 4:6.
- [11] LAUNDER, B. Second-moment closure: Present ... and future? *Int. J. Heat and Fluid Flow* 10 (1989), 282–300.
- [12] LAUNDER, B., AND SPALDING, D. The numerical computation of turbulent flows. *Computer Methods in Applied Mech. and Eng.* 3 (1974), 269–289.
- [13] LESCHZINER, M. Modelling engineering flows with Reynolds stress turbulence closure. *J. Wind Engng. and Ind. Aerodyn.* 35 (1991), 21–47.
- [14] LILLY, D. A proposed modification of the Germano subgrid-scale closure method. *Phys. Fluids A* 4 (1992), 633–635.
- [15] MOIN, P., AND KIM, J. Numerical investigation of turbulent channel flow. *J. Fluid Mech.* 118 (1982), 341–377.
- [16] NIELSEN, P. Specification of a two-dimensional test case. Report, ISSN 0902-7513 R9040, Dept. of Building Technology and Structural Engineering,, Aalborg Universitetscenter, Aalborg, 1990.
- [17] PATANKAR, S. *Numerical Heat Transfer and Fluid Flow*. McGraw-Hill, New York, 1980.
- [18] RENARD, J., AND GRESSER, D. Computational modelling of 2d hill flows. Diploma thesis. rept. 95/6, Thermo and Fluid Dynamics, Chalmers University of Technology, Gothenburg, 1995.
- [19] RESTIVO, A. *Turbulent Flow in Ventilated Rooms*. PhD thesis, University of London, Imperial College of Science and Technology, Mechanical Engineering Department, 1979.
- [20] SANDBERG, M. Velocity characteristics in mechanically ventilated office rooms. In *ROOMVENT -87* (Stockholm, 1987), vol. 2a.
- [21] SMAGORINSKY, J. General circulation experiments with the primitive equations. *Monthly Weather Review* 91 (1963), 99–165.
- [22] THOMPSON, B. Characteristics of a trailing-edge flow with turbulent boundary-layer separation. *Journal of Fluid Mechanics* 157 (1985), 305–326.
- [23] VAN DRIEST, E. On turbulent flow near a wall. *J. Aero. Sci.* 23 (1956), 1007–1011.
- [24] YANG, K.-S., AND FERZIGER, J. Large-eddy simulation of turbulent obstacle flow using a dynamic subgrid-scale model. *AIAA J.* 31 (1993), 1406–1413.